Grating Lobes Prediction in 3D Array Antennas

Sjoerd Bosma[†], Wessel P. Bruinsma[†], Robin P. Hes[†], Mark J. Bentum[‡], and Ioan E. Lager[†]
[†]Delft University of Technology, Faculty of Electrical Engineering, Mathematics and Computer Science,
Mekelweg 4, 2628 CD Delft, the Netherlands,
Emails: s.bosma-1@student.tudelft.nl, w.p.bruinsma@tudelft.nl, r.p.hes@student.tudelft.nl, i.e.lager@tudelft.nl
[‡]University of Twente, Faculty of Electrical Engineering, Mathematics and Computer Science,
7500 AE Enschede, the Netherlands, Email: m.j.bentum@utwente.nl

***Abstract*—This papers discusses an effective framework for determining the number and direction of all possible grating lobes in the case of three-dimensional (3D) array antennas. Illustrating examples support the introduced theoretical concepts. The analysis highlights some intrinsic benefits of using 3D architectures, when compared with planar arrays. It also presents incentives for including the discussion of this class of conceptually relevant systems in (under)graduate curricula.**

I. Introduction

The array antenna theory is elaborately treated in standard textbooks, e.g., [1], [2], for the case of linear and planar configurations. Surprisingly, three-dimensional (3D) array antennas receive (much) less attention: a general description of such arrays is given in [3, Section 10.2], some aspects concerning their synthesis are discussed in [4]–[6] and [7], [8] analyse their performance limits. Examples of practical implementations of 3D arrays are also scarce: the so-called crow's nest antennas [9]–[11], with the derived design reported in [12], and the broadband volumetric array studied in [13] (with an acoustic counterpart being described in [14]).

The progress in antenna technology and the advent of new applications, such as the Orbital Low Frequency ARray (OLFAR) distributed radio telescope [15], [16] are likely to change this situation. To fill in the conceptual gap, this paper highlights some basic, yet relevant features that substantiate the adequacy of 3D arrays for antenna applications. Its objective is building insight and, consequently, it focuses on the discussion of uniform array configurations. The main contribution is the detailed study of the onset of grating lobes (GLs) by establishing correspondences between the array lattice, on the one hand, and the scanning directions and the expected number and direction of pertaining GLs, on the other hand. This study will yield two important analytic results: (i) the smallest upper bound of the angle of the cone around the scanning direction within which no GL can occur and (ii) the number of GLs for a given scanning direction. These results may serve a purpose in the case of large, very loose, 3D arrays of the type that can be expected in space missions of the OLFAR type.

Apart from their technical applicability, the results established in this paper can provide opportune extensions to the material of (under)graduate antenna engineering curricula. In particular, the examples discussed in Section IV, illustrating global behaviours and features seldom touched upon in standard courses, are of special relevance.

After assembling the prerequisites, the paper will introduce a mechanism for determining the number and directions of the GLs. The theoretical framework will then be validated by means of illustrating numerical experiments. The paper will be finalised by drawing conclusions.

II. Prerequisites

A. Examined configuration

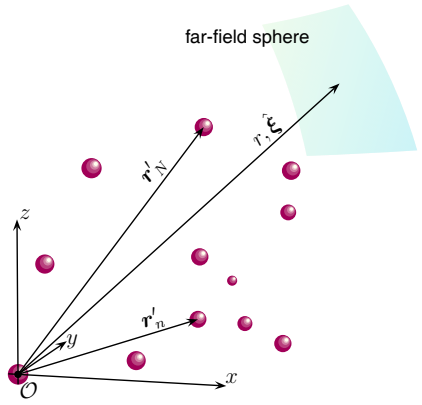

Fig. 1. 3D antenna array composed of isotropic radiators.

A general 3D array antenna is shown in Fig. 1. It consists of $N+1$ isotropic radiators $n = 0, \ldots, N$. Position in the configuration is specified by the coordinates $\{x, y, z\}$ with respect to a Cartesian reference frame with origin $\mathcal{O}$ and three mutually orthogonal base vectors $\{\hat{\boldsymbol{x}}, \hat{\boldsymbol{y}}, \hat{\boldsymbol{z}}\}$ of unit length each that, in this order, form a right-handed system. The position vector is $\boldsymbol{r} = x\hat{\boldsymbol{x}} + y\hat{\boldsymbol{y}} + z\hat{\boldsymbol{z}}$, with $|\boldsymbol{r}| = r$ and $\hat{\boldsymbol{\xi}} = \boldsymbol{r}/r$. The radiating elements' locations are denoted as $\boldsymbol{r}'_n$, $n = 0, \ldots, N$, with the reference element ($n = 0$) being located at $\mathcal{O}$. A spherical coordinate system with the same origin and coordinates $\{\vartheta, \varphi\}$ is also considered, ϑ measuring the tilting from $\hat{\boldsymbol{z}}$ and φ the trigonometric rotation from $\hat{\boldsymbol{x}}$. The elements' excitation is taken to be time-harmonic, with frequency f and angular frequency $\omega = 2\pi f$.

The array antenna radiates in free space, with electric permittivity ϵ_0, magnetic permeability μ_0 and wavespeed $c_0 = (\epsilon_0\mu_0)^{-½}$. Correspondingly, the wavenumber is $k_0 = \omega/c_0$ and the wavelength is $\lambda = c_0/f$.

B. Far-field radiation of 3D antenna arrays

In line with [17], the far-field electric field strength radiated in the observation direction $\hat{\boldsymbol{\xi}}(\vartheta, \varphi)$ by an array antenna is[1]

[1]This expression is habitually derived for planar arrays (see [1, Chapter 6], [2, Chapter 19]). Its validity can straightforwardly be extended to 3D arrays by observing that it is constructed using a *geometric projection* procedure.

$$\boldsymbol{E}(r,\hat{\boldsymbol{\xi}},\hat{\boldsymbol{\xi}}_{\mathrm{sc}}) = \frac{\boldsymbol{E}_{\mathrm{el}}^{\infty}(\hat{\boldsymbol{\xi}})}{4\pi r}\sum_{n=0}^{N} w_n \exp[-\mathrm{j}k_0(\hat{\boldsymbol{\xi}}-\hat{\boldsymbol{\xi}}_{\mathrm{sc}})\cdot\boldsymbol{r}'_n] \quad (1)$$

with $\boldsymbol{E}_{\mathrm{el}}^{\infty}(\hat{\boldsymbol{\xi}})$ being the far-field radiation characteristic of the *identical* elementary radiators, w_n some (complex) weights, and $\exp(\mathrm{j}k_0\hat{\boldsymbol{\xi}}_{\mathrm{sc}}\cdot\boldsymbol{r}'_n)$ representing the progressive phase, with $\hat{\boldsymbol{\xi}}_{\mathrm{sc}}(\vartheta_{\mathrm{sc}},\varphi_{\mathrm{sc}})$ being the scanning direction. The weights w_n are used for beam shaping purposes. Nonetheless, in many (space) applications preference is given to uniform elementary feeding [18], this implying that $w_n = 1$, which will be henceforth consistently assumed. Equation (1) evidences the standard factoring of the radiated field's expression into an elementary pattern $\boldsymbol{E}_{\mathrm{el}}^{\infty}(\hat{\boldsymbol{\xi}})$ and the array factor

$$\mathrm{AF}(\hat{\boldsymbol{\xi}},\hat{\boldsymbol{\xi}}_{\mathrm{sc}}) = \sum_{n=0}^{N}\exp[-\mathrm{j}k_0(\hat{\boldsymbol{\xi}}-\hat{\boldsymbol{\xi}}_{\mathrm{sc}})\cdot\boldsymbol{r}'_n]. \quad (2)$$

The array's radiation properties are examined via the directivity $D(\hat{\boldsymbol{\xi}})$ pattern on a sphere S_r in the far-field region [1, Section 2.5], [2, Section 15.2]. For the array factor, the directivity reads

$$D(\hat{\boldsymbol{\xi}}) = \frac{4\pi\left[\mathrm{AF}(\hat{\boldsymbol{\xi}})\,\mathrm{AF}^*(\hat{\boldsymbol{\xi}})\right]}{\int\limits_{S_r}\left[\mathrm{AF}(\hat{\boldsymbol{\xi}}')\,\mathrm{AF}^*(\hat{\boldsymbol{\xi}}')\right]\mathrm{d}\Omega} \quad (3)$$

with '*' denoting complex conjugation. The expression (3) is maximised in the direction in which fully constructive interference of the fields radiated by *all* elementary radiators occurs: in the scanning direction $\hat{\boldsymbol{\xi}}_{\mathrm{sc}}$, as directly following from (1) and (2) and, possibly, in the direction of the GLs.

III. Prediction of GL onset in uniform 3D antenna arrays

The quality of the array antenna's radiation pattern is given by the sidelobes level (SLL) and beamwidth, (usually) under the provision of a GL-free operation. Note that, unlike in the case of planar arrays[2], there seems to exist no alternative to the full evaluation of (3) for examining the radiation pattern's features and metrics.

As concerns the onset of GLs, it is important to predict their number and directions. While a general treatment of this problem requires a comprehensive study based on (2), uniformly-fed, uniform array antennas can be effectively analyzed by means of the henceforth described framework. Note that this analysis is confined to the onset of GLs in the visible space.

Let the case of an array antenna consisting of isotropic radiators located at

$$\boldsymbol{r}'_{n_x,n_y,n_z} = n_x(\kappa_x\lambda/2)\hat{\boldsymbol{x}} + n_y(\kappa_y\lambda/2)\hat{\boldsymbol{y}} + n_z(\kappa_z\lambda/2)\hat{\boldsymbol{z}} \quad (4)$$

where $n_\alpha = 0,\ldots,N_\alpha$ and $\kappa_\alpha\in\mathbb{R}$, $\kappa_\alpha > 1$, with $\alpha = x,y,z$. The numbers N_α are taken to be larger than zero for ensuring that the examined 3D arrays are non-degenerate. Substitution of (4) in (2) then yields

$$\begin{aligned}\mathrm{AF}(\hat{\boldsymbol{\xi}},\hat{\boldsymbol{\xi}}_{\mathrm{sc}}) &= \sum_{n_x=0}^{N_x}\sum_{n_y=0}^{N_y}\sum_{n_z=0}^{N_z}\exp\left[-\mathrm{j}k_0(\hat{\boldsymbol{\xi}}-\hat{\boldsymbol{\xi}}_{\mathrm{sc}})\cdot\boldsymbol{r}'_{n_\alpha}\right]\\ &= \mathrm{AF}_x(\hat{\boldsymbol{\xi}},\hat{\boldsymbol{\xi}}_{\mathrm{sc}})\,\mathrm{AF}_y(\hat{\boldsymbol{\xi}},\hat{\boldsymbol{\xi}}_{\mathrm{sc}})\,\mathrm{AF}_z(\hat{\boldsymbol{\xi}},\hat{\boldsymbol{\xi}}_{\mathrm{sc}}) \quad (5)\end{aligned}$$

with

$$\mathrm{AF}_\alpha(\hat{\boldsymbol{\xi}},\hat{\boldsymbol{\xi}}_{\mathrm{sc}}) = \sum_{n_\alpha=0}^{N_\alpha}\exp[-\mathrm{j}\pi\kappa_\alpha n_\alpha(\hat{\boldsymbol{\xi}}-\hat{\boldsymbol{\xi}}_{\mathrm{sc}})\cdot\hat{\boldsymbol{\alpha}}], \quad \text{for } \alpha = x,y,z \text{ and } \hat{\boldsymbol{\alpha}} = \hat{\boldsymbol{x}},\hat{\boldsymbol{y}},\hat{\boldsymbol{z}}. \quad (6)$$

The onset of GLs requires fully constructive interference in directions $\hat{\boldsymbol{\xi}}\neq\hat{\boldsymbol{\xi}}_{\mathrm{sc}}$. From (6), $\pi\kappa_\alpha n_\alpha(\hat{\boldsymbol{\xi}}-\hat{\boldsymbol{\xi}}_{\mathrm{sc}})\cdot\hat{\boldsymbol{\alpha}}$ must then be a multiple of 2π for any n_α, this entailing the condition

$$\kappa_\alpha(\hat{\boldsymbol{\xi}}-\hat{\boldsymbol{\xi}}_{\mathrm{sc}})\cdot\hat{\boldsymbol{\alpha}} = 2u_\alpha, \text{ with } u_\alpha\in\mathbb{Z} \quad (7)$$

with at least one u_α being necessarily nonzero. The existence of u_α such that (7) is satisfied is a *necessary and sufficient condition* for fully constructive interference in the $\hat{\boldsymbol{\xi}}\neq\hat{\boldsymbol{\xi}}_{\mathrm{sc}}$ direction. From (7) it directly follows that

$$\hat{\boldsymbol{\xi}} = 2\boldsymbol{\zeta} + \hat{\boldsymbol{\xi}}_{\mathrm{sc}} \quad (8)$$

with $\boldsymbol{\zeta} = \sum_\alpha u_\alpha/\kappa_\alpha\hat{\boldsymbol{\alpha}}$. Note that u_α uniquely determine the relevant $\hat{\boldsymbol{\xi}}$. Moreover, since $\|\hat{\boldsymbol{\xi}}\| = \|\hat{\boldsymbol{\xi}}_{\mathrm{sc}}\| = 1$, the triangle inequality ensures that $\|\boldsymbol{\zeta}\|\leqslant 1$. From (8), the directions of GLs for a given $\hat{\boldsymbol{\xi}}_{\mathrm{sc}}$ are given by all combinations $\{\boldsymbol{\zeta},\hat{\boldsymbol{\xi}}_{\mathrm{sc}}\}$ verifying $\|2\boldsymbol{\zeta}+\hat{\boldsymbol{\xi}}_{\mathrm{sc}}\| = 1$. Conversely, all scanning directions $\hat{\boldsymbol{\xi}}_{\mathrm{sc}}$ for which a given $\boldsymbol{\zeta}$ corresponds to a GL satisfy (8).

The condition $\|\boldsymbol{\zeta}\|\leqslant 1$ requires that $|u_\alpha|\leqslant\kappa_\alpha$, that, in turn, implies that the number of nontrivial $\boldsymbol{\zeta}-$s is less than $\left[\Pi_\alpha(2\kappa_\alpha+1)\right]-1 = O(\kappa_x\kappa_y\kappa_z)$, with O denoting the Landau order symbol [19, Appendix A.8]. The directions of all GLs for a given $\hat{\boldsymbol{\xi}}_{\mathrm{sc}}$ can then be computed in $O(\kappa_x\kappa_y\kappa_z)$ steps of constant time complexity.

By accounting for the fact that $\|\hat{\boldsymbol{\xi}}\| = \|\hat{\boldsymbol{\xi}}_{\mathrm{sc}}\| = 1$, (8) yields

$$\|\boldsymbol{\zeta}\|^2 + \hat{\boldsymbol{\xi}}_{\mathrm{sc}}\cdot\boldsymbol{\zeta} = 0. \quad (9)$$

The locus of the solutions of (9) is the intersection of the unit sphere centred at the origin with a plane orthogonal to $\boldsymbol{\zeta}$ and passing through $-\boldsymbol{\zeta}$. Moreover, this intersection is a circle of radius $\left(1-\|\boldsymbol{\zeta}\|^2\right)^{\frac{1}{2}}$. It is interesting to note that this circle collapses to a single point, thus a single scanning direction, when $\|\boldsymbol{\zeta}\| = 1$, with the scanning direction and the GL's direction being, in this case, opposite. Such examples will be shown in Section IV-B. Equation (9), corroborated with the condition $\|\boldsymbol{\zeta}\|\leqslant 1$, allows determining *all* possible GLs for a given array and scanning direction $\hat{\boldsymbol{\xi}}_{\mathrm{sc}}$. This equation lends itself to an effective numerical treatment due to the fact that it only needs being solved for an $O(\kappa_x\kappa_y\kappa_z)$, *finite* number of combinations of integers u_x,u_y,u_z.

From (8) and (9) it follows that

$$\hat{\boldsymbol{\xi}}_{\mathrm{sc}}\cdot\hat{\boldsymbol{\xi}} = 1-2\|\boldsymbol{\zeta}\|^2 \leqslant 1-2/\kappa^2 \quad (10)$$

with $\kappa = \max(\kappa_x,\kappa_y,\kappa_z)$. This entails that the angle between the scanning direction and a corresponding GL direction is $\arccos(1-2\|\boldsymbol{\zeta}\|^2)$, the minimum angle being $\gamma_\kappa = \arccos(1-2/\kappa^2)$. Furthermore, let $\hat{\boldsymbol{\xi}}_1 = 2\boldsymbol{\zeta}_1+\hat{\boldsymbol{\xi}}_{\mathrm{sc}}$ and $\hat{\boldsymbol{\xi}}_2 = 2\boldsymbol{\zeta}_2+\hat{\boldsymbol{\xi}}_{\mathrm{sc}}$

[2]For example, broadside scanned, planar arrays can be effectively examined by invoking the ingenious analysis strategy in [3, p. 254].

be the directions of two different GLs. Then from (8) and (9) it follows that

$$\hat{\boldsymbol{\xi}}_1 \cdot \hat{\boldsymbol{\xi}}_2 = 1 - 2\|\boldsymbol{\zeta}_1 - \boldsymbol{\zeta}_2\|^2 \leqslant 1 - 2/\kappa^2 \qquad (11)$$

implying that the angle between the directions of two GLs is $\arccos(1 - 2\|\boldsymbol{\zeta}_1 - \boldsymbol{\zeta}_2\|^2)$, its minimum value being again γ_κ. The inequalities in (10) and (11) define a cone around each GL direction within which no other GL can occur. This cone corresponds to a solid angle of *at least* $\Omega = 2\pi[1-\cos(\gamma_\kappa/2)]$ steradians that, in turn, shows that the number of GLs for a particular scanning direction is bounded from above by $4\pi/\Omega - 1 \leqslant 4\kappa^2 - 1$. It can now be stated that the number of GLs for a particular scanning direction is $O(\kappa^2)$.

It can now be concluded that the maximum element spacing factor κ introduced in (10) provides an opportune measure of the number of GLs corresponding to a 3D array antenna with elements on a uniform lattice. As expected, a larger κ will imply that there will be more scanning directions for which GLs occur or, reciprocally, more GLs per scanning direction.

IV. Illustrative Experiments

The radiation features of 3D array antennas are illustrated by means of a number of representative cases. For conceptual clarity, the analysis in this paper is confined to 3D uniform arrays, with examples concerning non-uniform arrays being available in [20]. Triplets $p_x \times p_y \times p_z$ are henceforth used for indicating lattice parameters in the $\hat{\boldsymbol{x}}, \hat{\boldsymbol{y}}, \hat{\boldsymbol{z}}$ directions, in this order. All examined arrays consist of $5 \times 5 \times 4$ elements.

A. Examples of radiation patterns of 3D array antennas

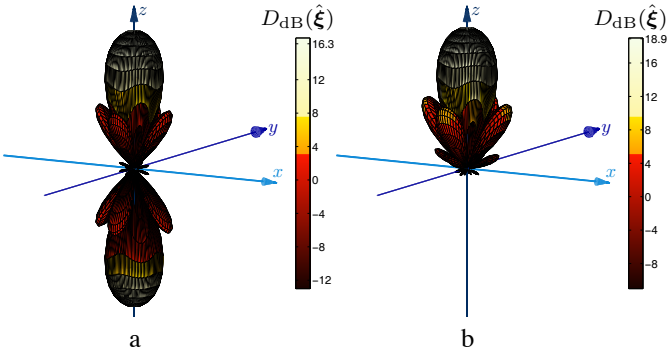

Fig. 2. Directivity patterns for (a) $\lambda/2 \times \lambda/2 \times \lambda/2$ spaced and (b) $\lambda/2 \times \lambda/2 \times \lambda/4$ spaced arrays. The beam is scanned at $\hat{\boldsymbol{\xi}}_{\mathrm{sc}}(0°, 0°)$.

The radiation of $\lambda/2 \times \lambda/2 \times \lambda/2$ and $\lambda/2 \times \lambda/2 \times \lambda/4$ spaced array antennas is shown in Fig. 2. The beam is scanned at $\hat{\boldsymbol{\xi}}_{\mathrm{sc}}(0°, 0°)$. The plots evidence a peak SLL that is in line with the well known $-13.46\,\mathrm{dB}$ level [1, Section 6.3]. In principle, no GLs are observed, the beam pointing towards $-\hat{\boldsymbol{z}}$ in Fig. 2.a being an effect of the configuration's symmetry, as it would also be the case with planar arrays. Nevertheless, when interpreting the 3D array as a 5×5, $\hat{\boldsymbol{x}}, \hat{\boldsymbol{y}}$-oriented, uniform planar array consisting of $\hat{\boldsymbol{z}}$-oriented, uniform, linear arrays consisting of 4 elements, the beam pointing towards $-\hat{\boldsymbol{z}}$ can be also interpreted as a superposition of the intrinsic GL of the relevant endfire, linear arrays. From this perspective, the lobe can then be construed as an array GL, this aspect playing later a role in this analysis. When turning to the pattern in Fig. 2.b, it demonstrates a specific 3D array capability, namely that a one-sided radiation can be obtained by placing an *even* number of elements at $\lambda/4$ in the $\hat{\boldsymbol{z}}$ direction.

The beam scanning is examined in Fig. 3 for the case of the $\lambda/2 \times \lambda/2 \times \lambda/2$ spaced array. As expected, the beam broadens and the SLL is affected. The plots evidence another specific 3D array feature, namely breaking the radiation's symmetry with respect to the $z = 0$ plane as a result of the phase shift in the $\hat{\boldsymbol{z}}$ direction. No GLs are observed.

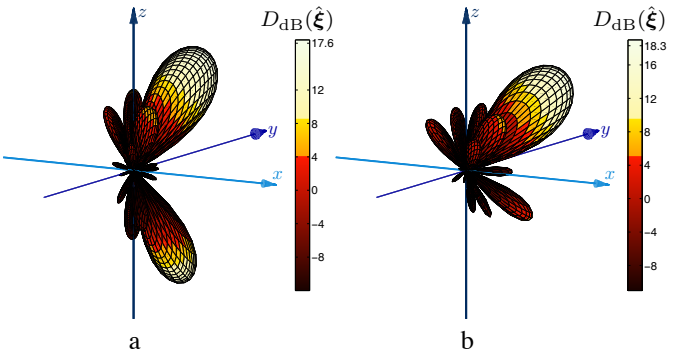

Fig. 3. Directivity patterns for a $\lambda/2 \times \lambda/2 \times \lambda/2$ spaced array antenna. (a) Beam scanned at $\hat{\boldsymbol{\xi}}_{\mathrm{sc}}(30°, 30°)$; (b) beam scanned at $\hat{\boldsymbol{\xi}}_{\mathrm{sc}}(45°, 30°)$.

Finally, a $\lambda \times \lambda \times \lambda$ spaced array antenna is examined (see Fig. 4). A first observation is that the beamwidth scales down with increasing array size, this corroborating with the situation of linear and planar arrays [21]. The peak SLL again deviates from the $-13.46\,\mathrm{dB}$ level. The wide inter-element spacing results in the onset of GLs. By again taking the 3D configuration to be a uniform, planar array of uniform, endfire, linear arrays, the onset of GLs can be attributed to both the linear and the planar arrays being undersampled. As when the beam is scanned, the skew[3] scanning results in an intricate pattern, with some GLs being suppressed. This is a unique feature of 3D array antennas that clearly differentiates them from their planar counterparts.

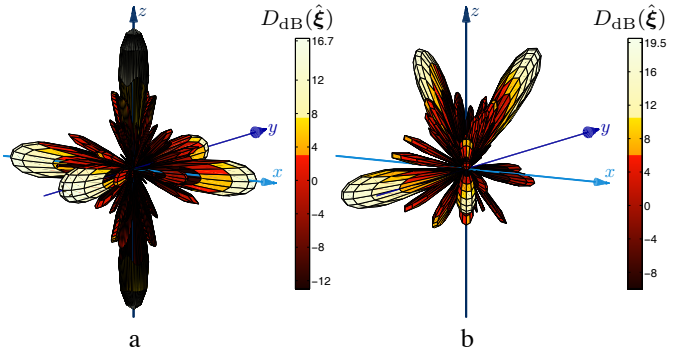

Fig. 4. Directivity patterns for a $\lambda \times \lambda \times \lambda$ spaced array antenna. (a) Beam scanned at $\hat{\boldsymbol{\xi}}_{\mathrm{sc}}(0°, 0°)$; (b) beam scanned at $\hat{\boldsymbol{\xi}}_{\mathrm{sc}}(30°, 30°)$.

[3]Not parallel with at least one of the lattice's edges.

B. Prediction of the GLs onset in the case of 3D array antennas

The 3D array antennas examined in Section IV-A are now used for demonstrating the validity of the GLs number and direction detecting algorithm discussed in Section III. The results are collected in Table I, the cases being specified by indicating their pertaining radiation patterns. The algorithm correctly identified all GLs and their corresponding directions. Note that the algorithm identifies the lobe pointing towards $-\hat{\boldsymbol{z}}$ in Fig. 2.a as a GL, this being consistent with the above discussion of the relevant plot.

TABLE I. GL ANALYSIS FOR THE EXAMINED ARRAY ANTENNAS.

Radiation pattern	Beam scanning	GLs number	GLs directions
Fig. 2.a	$(0°, 0°)$	1	$(180°, 0°)$
Fig. 3.a	$(30°, 30°)$	0	–
Fig. 3.b	$(45°, 30°)$	0	–
Fig. 4.a	$(0°, 0°)$	5	$(90°, 0°)$, $(90°, 90°)$, $(90°, 180°)$, $(90°, 270°)$, $(180°, 0°)$
Fig. 4.b	$(30°, 30°)$	0	–

The algorithm's correctness was further checked by making a full analysis of the $\lambda \times \lambda \times \lambda$ spaced array antenna for scanning angles $0 < \vartheta < 90°$ and $0 < \varphi < 45°$. As expected, the algorithm detected in most cases *no* GLs, this corroborating with the array being scanned at skew angles. The only exception was represented by the case of scanning at $\hat{\boldsymbol{\xi}}_{\rm sc}(45°, 45°)$, when 3 GLs were found at $(45°, 135°)$, $(45°, 215°)$ and $(45°, 315°)$, respectively. Clearly, this situation is a consequence of the symmetry induced by the coincidence of a cubic lattice and a $\hat{\boldsymbol{\xi}}_{\rm sc}(45°, 45°)$ scanning. It must, however, be noted that while, strictly speaking, the radiation patterns displayed no GLs, they did evidence very high lobes, their level being in some cases just marginally under that of the main lobe. These high lobes are, in fact, vestiges of the original GLs, (slightly) tapered by the skew scanning of the 3D array antennas.

Let now the case of a more general uniform, orthogonal, 3D array. The lattice spacing is $\kappa_x\lambda/2$, $\kappa_y\lambda/2$ and $\kappa_z\lambda/2$ in the x, y and z directions, respectively. The numbers N_x, N_y and N_z are arbitrary and finite. The framework in Section III is used for examining the correlation between the parameters $\{\kappa_x, \kappa_y, \kappa_z\}$, the scanning direction $\hat{\boldsymbol{\xi}}_{\rm sc}$ and the number of GLs. The $\hat{\boldsymbol{\xi}}_{\rm sc}$-s for which at least one GL is onset are shown in Fig. 5. Note that the curves collapse to isolated points for $\arccos(\hat{\boldsymbol{\xi}}_{\rm GL} \cdot \hat{\boldsymbol{\xi}}_{\rm sc}) = \pi$, as anticipated in the discussion of (9). Due to the duality $\hat{\boldsymbol{\xi}}_{\rm sc} \leftrightarrow$ GL direction $\hat{\boldsymbol{\xi}}_{\rm GL}$, the figures clearly illustrate the correspondence between the number of GLs and the pertaining $\hat{\boldsymbol{\xi}}_{\rm sc}$, with any intersection of curves indicating the simultaneous onset of more GLs. In the cases depicted in Fig. 5.a and b only single GLs occur. Nevertheless, Fig. 5.c shows 3 GLs appearing when scanning at $\vartheta \in \{45°, 135°\}$ and $\varphi \in \{45°, 135°, 225°, 315°\}$. The situation in Fig. 5.d is even more intricate. Note that this analysis focuses on *genuine* GLs, 'near-GLs' being construed as sidelobes, as it should be. Figure 5 also illustrates the opposite behaviours of the radius of the locus of the solutions of (9) (circles in 3D) and the minimum angle between a $\hat{\boldsymbol{\xi}}_{\rm sc}$ and a corresponding GL. Concretely, the largest possible angle (π) corresponds to circles degenerated to a single point, whereas lower values correspond to increasingly larger circles - bear in mind that the aspect of the plots is influenced by the distortions that are inherent to the spherical to planar transformation.

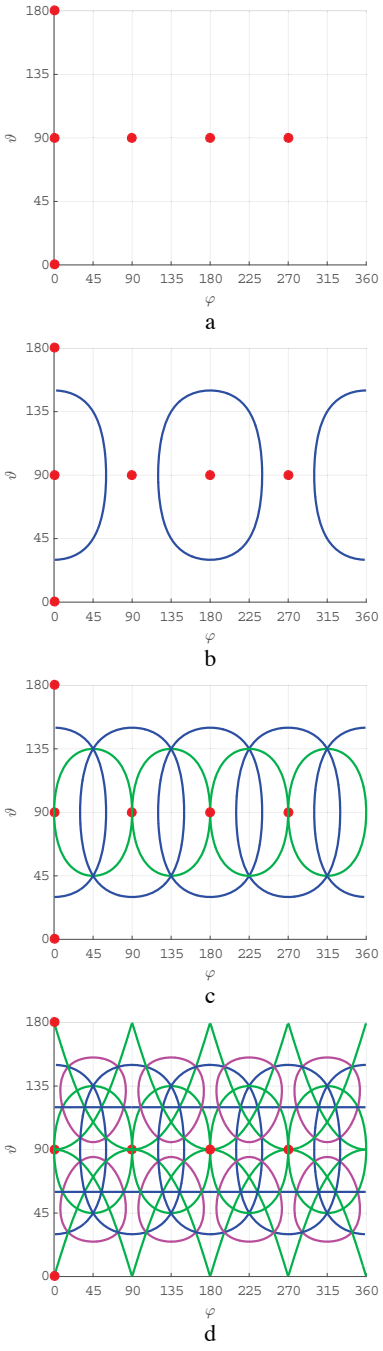

Fig. 5. Scanning direction $\hat{\boldsymbol{\xi}}_{\rm sc} \leftrightarrow$ GL correspondence for different lattice spacing. (a) $\{\kappa_x, \kappa_y, \kappa_z\} = \{1, 1, 1\}$; (b) $\{\kappa_x, \kappa_y, \kappa_z\} = \{2, 1, 1\}$; (c) $\{\kappa_x, \kappa_y, \kappa_z\} = \{2, 2, 1\}$; (d) $\{\kappa_x, \kappa_y, \kappa_z\} = \{2, 2, 2\}$. The colours correspond to the following cases: red – $\arccos(\hat{\boldsymbol{\xi}}_{\rm GL} \cdot \hat{\boldsymbol{\xi}}_{\rm sc}) = \pi$; blue – $\arccos(\hat{\boldsymbol{\xi}}_{\rm GL} \cdot \hat{\boldsymbol{\xi}}_{\rm sc}) = \pi/3$; green – $\arccos(\hat{\boldsymbol{\xi}}_{\rm GL} \cdot \hat{\boldsymbol{\xi}}_{\rm sc}) = \pi/2$; pink – $\arccos(\hat{\boldsymbol{\xi}}_{\rm GL} \cdot \hat{\boldsymbol{\xi}}_{\rm sc}) = 2\pi/3$, with $\hat{\boldsymbol{\xi}}_{\rm GL}$ being the GL direction.

V. EDUCATIONAL RELEVANCE OF THE ANALYSIS

The theoretical construction in Section III and the numerical experiments reported in Section IV provide opportune ex-

tensions to the material of (under)graduate antenna engineering curricula. Here, it should be noted that antenna courses commonly exemplify the GL performance for particular lattice and scanning direction combinations. The hereby presented results, especially those in Table I and Fig. 5, offer an extremely instructive *global* performance perspective. Furthermore, the skew scanning shown in Fig. 4 offers credible arguments for a less evident possibility to suppress the onset of GL in 'planar' arrays whose elements are themselves linear arrays.

VI. Conclusions

Some characteristic features of the radiation from three-dimensional (3D) array antennas were discussed. An effective framework for studying and/or calculating the number and direction of all possible grating lobes (GLs) was assembled. Two important analytic results concerning uniform, orthogonal, 3D arrays were derived: (i) the angle of the cone around the scanning direction withing which no GL can occur is bounded from above by $\arccos(1-2/\kappa^2)$, with κ representing the maximum ratio between the lattice spacing in any of the x, y or z directions and $\lambda/2$, with λ denoting the free space wavelength at the operating frequency; (ii) the expected number of GLs for a given scanning direction is of order κ^2. These results may be of relevance for large, very loose, 3D arrays of the type that can be expected in space missions of the OLFAR type.

The analytical apparatus was then validated via a number of simple, yet illustrating numerical examples. At the same time, these numerical experiments cogently demonstrated the favourable radiation properties of (uniform) 3D arrays, with specific features that cannot be obtained with planar arrays. In particular, it has been shown that skew beam scanning in 3D arrays can preclude the GL onset in specific configurations.

References

[1] C. A. Balanis, *Antenna Theory: Analysis and Design*, 4th ed., New York: John Wiley & Sons Inc., 2016.

[2] S. J. Orfanidis, *Electromagnetic Waves and Antennas*, [Online]. Available: www.ece.rutgers.edu/orfanidi/ewa.

[3] H. J. Visser, *Array and Phased Array Antenna Basics*, Hoboken, NJ: John Wiley & Sons Inc., 2005.

[4] R. Voles, "Spherical shell and volume arrays," *IEE Proc-H*, vol. 142, no. 6, pp. 498–500, Dec. 1995.

[5] J. M. Rigelsford and A. Tennant, "A synthetic acoustic volumetric array," in *Proc. SAM 2006*, Waltham, MA, Jul. 2006, pp. 313–314.

[6] J. M. Rigelsford and A. Tennant, "Sidelobe reduction in a random spherical volumetric array using frequency diversity," *Applied Acoustics*, vol. 74, no. 6, pp. 865–869, Jun. 2013.

[7] D. T. Vu, A. Renaux, R. Boyer, and S. Marcos, "Performance analysis of 2D and 3D antenna arrays for source localization," in *Proc. 1^{th} EUSIPCO-2010*, Aalborg, Denmark, Aug. 2010, pp. 661–665.

[8] D. T. Vu, A. Renaux, R. Boyer, and S. Marcos, "A Cramér Rao bounds based analysis of 3D antenna array geometries made from ULA branches," *Multidim Syst Sign Process*, vol. 24, no. 1, pp. 121–155, Mar. 2013.

[9] H. Wilden, "Crow's-nest antenna," *Electron. Lett.* vol. 16, no. 7, pp. 256–257, Mar. 1980.

[10] H. Wilden and J. Ender, "The crow's-nest antenna - special aspects and results," in *Proc. 17^{th} EuMC*, Rome, Italy, Sep. 1987, pp. 509–514.

[11] H. Wilden and J. Ender, "The crow's nest antenna – experimental results," in *Rec. IEEE 1990 International Radar Conference*, Arlington, VA, May 1990, pp. 280–285.

[12] J. A. Scholz, "Volumetric phased array antenna system," US Patent 6,636,177 B1, Oct. 21, 2003.

[13] A. Tennant, A. F. Fray, D. B. Adamson, and M. W. Shelley, "Beam scanning characteristics of 64 element broadband volumetric array," *Electron. Lett.* vol. 33, no. 24, pp. 2001–2002, Nov. 1997.

[14] J. M. Rigelsford and A. Tennant, "A 64 element acoustic volumetric array," *Applied Acoustics*, vol. 61, no. 4, pp. 469–475, Dec. 2000.

[15] R. T. Rajan, S. Engelen, M. J. Bentum, and C. J. M. Verhoeven, "The Orbiting Low Frequency Antenna Array," in *Proc. of the IEEE Aerospace*, Big Sky, Montana, USA, March. 2011.

[16] P. K. A. van Vugt, A. Meijerink and M. J. Bentum, "Calibration Approach of the OLFAR Space Based Radio Telescope," in *Proc. of the 65^{th} International Astronautical Congress*, Toronto, Canada, Sep. 2014.

[17] I. E. Lager and M. Simeoni, "Radiation properties of non-uniform array antennas," in *Proc. 42^{nd} EuMC*, Amsterdam, the Netherlands, Oct.-Nov. 2012, pp. 502–505.

[18] M. C. Viganó, G. Toso, G. Caille, C. Mangenot, and I. E. Lager, "Sunflower array antenna with adjustable density taper," *IJAP*, vol. 2009, Article ID 624035, Jan. 2009.

[19] A. T. de Hoop, *Handbook of Radiation and Scattering of Waves*, London: Academic Press, 1995, xxx + 1085 pp.; electronic reproduction (with corrections) 2008, freely downloadable, for private use, from http://www.atdehoop.com.

[20] M. J. Bentum, I. E. Lager, S. Bosma, W. P. Bruinsma, and R. P. Hes, "Beamforming in sparse, random, 3D array antennas with fluctuating element locations," in *Proc. 9^{th} EuCAP*, Lisbon, Portugal, Apr. 2015.

[21] C. I. Coman, I. E. Lager, and L. P. Ligthart, "Design considerations in sparse array antennas," in *Proc. 3^{rd} EuRAD*, Manchester, UK, Sep. 2006, pp. 72–75.